IEEE Access
Multidisciplinary | Rapid Review | Open Access Journal

Received January 18, 2019, accepted February 25, 2019, date of publication March 4, 2019, date of current version March 25, 2019.

Digital Object Identifier 10.1109/ACCESS.2019.2902844

Reconfigurable Microstrip Magnetic Dipole Antenna With Switchable Conical Beams for Aerial Drone Applications

ZHIXI LIANG, (Member, IEEE), ZHIPENG LIANG, YUANXIN LI, (Member, IEEE), JUHUA LIU, (Member, IEEE), JIAYIN QIN, AND YUNLIANG LONG, (Senior Member, IEEE)
School of Electronics and Information Technology, Sun Yat-sen University, Guangzhou 516001, China

Corresponding author: Yuanxin Li (liyuanx@mail.sysu.edu.cn)

This work was supported in part by the Natural Science Foundation of China under Grant 61701549, and in part by the China Postdoctoral Science Foundation under Grant 2017M612788.

ABSTRACT A novel reconfigurable microstrip magnetic dipole antenna with switchable conical beams is proposed for aerial drone applications. The proposed antenna consists of three sub-cavities that are separated by two groups of shorting posts. To reconfigure the resonant cavities, a number of p-i-n diodes are connected to the shorting posts and are used as RF switches. The antenna is capable of resonating in three different operating states. The theoretical analysis shows that the three resonant modes produce conical beams with different elevation angles. The reconfigurable microstrip magnetic dipole antenna yields an overlapping bandwidth from 2.39 to 2.49 GHz for WLAN 2.4-GHz application and produces switchable conical beams for different operating states. The peak gain is 3.9, 4.0, and 4.3 dBi, respectively, when the elevation angle is 90°, 66°, and 54°. The conical beams have omnidirectional radiation patterns in the azimuth plane for the elevation angles. The proposed antenna shows promise for improving the transmission of aerial drones operating at varying altitudes.

INDEX TERMS Reconfigurable antenna, microstrip magnetic dipole, beam steering, conical beam.

I. INTRODUCTION

The development of aerial drones has captured a lot of attention due to their widespread applications, such as aerial photography, event monitoring, and delivery of goods. Regardless of the application or the size of the drones, antennas are necessary for remote control and data transmission. Electric monopole antennas are widely used in drones because they have omnidirectional radiation patterns in the azimuth plane. Most drones operate at altitudes below 200 meters. When they are flying at different altitudes, as shown in Fig. 1, the elevation angle from the drone to the ground controller varies. However, a conventional monopole antenna produces a conical beam with a fixed elevation angle, which limits the coverage area of the antenna. To improve the transmission between the aerial drone and the ground controller, a beam-steering antenna is a promising solution.

In the recent decade, many reconfigurable antennas have been proposed with different beam-steering techniques. Reconfigurable parasitic elements [1]–[4] and frequency selective surfaces (FSS) [5]–[7] are widely used in beam-steering antennas. They are arranged as directors or reflectors to steer the main beam in different directions. Leaky-wave antennas are good candidates for beam-steering applications because their main beam can be frequency controlled. By loading switchable shorting vias [8], [9] or lumped elements [10], fixed-frequency beam-scanning leaky-wave

FIGURE 1. Scheme of the wireless transmission between the ground controller and the aerial drones at different altitudes.

The associate editor coordinating the review of this manuscript and approving it for publication was Raghvendra Kumar Chaudhary.

antennas are obtained. Beam steering is also achieved by employing an asymmetrical arrangement of the PIN diodes on a symmetrical structure [11], [12]. However, most of the beam-steering reconfigurable antennas produce directional radiation, which does not provide stable coverage for all azimuth directions.

Recently, several reconfigurable patch antennas [13]–[16] were reported to achieve switchable broadside and conical radiation for indoor wireless applications. Different radiation patterns are achieved by using the monopolar patch and normal patch modes of the square [14], [15], circular [16], or square-ring [13] patches. However, the elevation angles of the conical beams produced by these antennas are less than 50°. The small elevation angle limits the transmission distance for drone applications.

Microstrip magnetic dipole antennas [17], [18] were first proposed to design low-profile vertically polarized Yagi arrays. They provide an omnidirectional radiation pattern similar to that of an electric dipole and can be implemented to design omnidirectional circular polarized antennas [19], [20]. In this paper, a novel microstrip magnetic dipole antenna with switchable conical beams is proposed. The conical beams with different elevation angles are produced by different resonant modes of the microstrip magnetic dipole antenna. The radiation patterns of these resonant modes are analyzed in Section II. The antenna configuration is depicted in Section III. The parameter study in Section IV is conducted to show the design process of the proposed antenna. The measurement and comparison are discussed in Section V.

II. THORETICAL ANALYSIS

As shown in Fig. 2, the microstrip magnetic dipole antenna has a low-profile rectangular cavity, consisting of two planar conductors and three shorting sidewalls. It is assumed that the thickness h is very small compared to the wavelength in the free space, and much less than the cavity length L and width W.

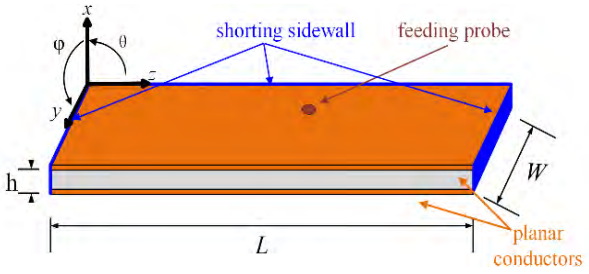

FIGURE 2. Geometry of the microstrip magnetic dipole antenna.

As shown in Fig. 3(a), the region between the two planar conductors can be treated as a cavity bounded by a magnetic sidewall of perfect magnetic conductor (PMC) and three electric sidewalls of perfect electric conductor (PEC). As depicted in Fig. 3(b), the theoretical model can be regarded as a section of a rectangular waveguide (ADD'A') bisected by a magnetic wall (BC).

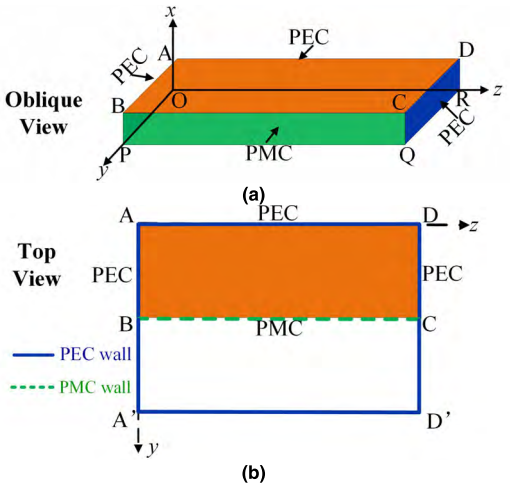

FIGURE 3. Cavity model of the microstrip magnetic dipole antenna. (a) Oblique view. (b) Top view.

A. TM^x MODES OF THE RECTANGULAR WAVEGUIDE

The close proximity between the two planar conductors suggests that the electric field only consists of the x-component and thus the magnetic field has only yz-components in the region bounded by the planar conductors. Therefore, the modes supported by the cavity model are transverse magnetic with respect to the x-direction (TM^x). The electro-magnetic field inside the cavity can be expanded in terms of the TM$^x_{mn}$ mode of the corresponding rectangular waveguide. For TM$^x_{mn}$ modes of the conventional rectangular waveguide, the transverse magnetic fields are characterized by $H_x = 0$ and the solution of E_x can be found by solving the Helmholtz wave equation [21]:

$$\begin{aligned} E_x &= A_{mn} \sin(\frac{m\pi y}{2W}) \sin(\frac{n\pi z}{L}) e^{-j\beta x} \\ m &= 1, 2, 3 \ldots \text{ and } n = 1, 2, 3 \ldots \end{aligned} \tag{1}$$

where A_{mn} is the amplitude constant for TM$^x_{mn}$ modes, β is the propagation constant. Other transverse magnetic field components can be obtained from the simplified Maxwell's equation for TM$^x_{mn}$ modes [22]:

$$\begin{cases} H_y = \dfrac{j\omega\varepsilon}{k_c^2} \dfrac{\partial E_x}{\partial z} \\ \quad = A_{mn} \dfrac{j\omega\varepsilon}{k_c^2} (\dfrac{n\pi}{L}) \sin(\dfrac{m\pi y}{2W}) \cos(\dfrac{n\pi z}{L}) e^{-j\beta x} \\ H_z = -\dfrac{j\omega\varepsilon}{k_c^2} \dfrac{\partial E_x}{\partial y} \\ \quad = -A_{mn} \dfrac{j\omega\varepsilon}{k_c^2} (\dfrac{m\pi}{2W}) \cos(\dfrac{m\pi y}{2W}) \sin(\dfrac{n\pi z}{L}) e^{-j\beta x} \end{cases} \tag{2}$$

where $k_c = \sqrt{k^2 - \beta^2}$ is the cutoff wavenumber, and $k = \omega\sqrt{\mu\varepsilon}$ is the wavenumber of the dielectric material inside the cavity. $\mu = \mu_0\mu_r$ and $\varepsilon = \varepsilon_0\varepsilon_r$ are the permeability and permittivity of the dielectric material, respectively.

B. TM^x MODES OF THE MICROSTRIP MAGNETIC DIPOLE

If the microstrip magnetic dipole antenna supports these modes, their mode functions (2) should meet the boundary condition of the PMC wall (BCQP):

$$H_z|_{y=W} = 0 \tag{3}$$

The boundary conditions are satisfied when m is an odd number. Therefore, the microstrip magnetic dipole antenna supports the TM^x_{mn} modes, where m = 1, 3, 5…, n = 1, 2, 3…From the constraint equation:

$$(\frac{m\pi}{2W})^2 + (\frac{n\pi}{L})^2 = k^2 = (2\pi f)^2\mu\varepsilon \tag{4}$$

we obtain the resonant frequencies for the supported TM^x_{mn} modes:

$$f_{mn}^{TM} = \frac{1}{2\pi\sqrt{\mu\varepsilon}}\sqrt{(\frac{m\pi}{2W})^2 + (\frac{n\pi}{L})^2} \quad \begin{vmatrix} m = 1, 3, 5\ldots \\ n = 1, 2, 3\ldots \end{vmatrix} \tag{5}$$

If the antenna length L is more than twice of the width W, $f_{11}^{TM} < f_{12}^{TM} < f_{13}^{TM} < f_{31}^{TM}$ is satisfied. In this work the microstrip magnetic dipole antenna is designed to resonate in the TM^x_{11}, TM^x_{12}, and TM^x_{13} modes at its three lowest resonant frequencies when choosing a large L $(L>2W)$.

C. FAR-FIELD OF THE MICROSTRIP MAGNETIC DIPOLE

The radiation of the microstrip magnetic dipole antenna is mainly contributed by the open edge. The radiating edge can be replaced by an equivalent magnetic current $\vec{M}$. If the thickness h is much less than the wavelength, the effect of the shorting sidewalls on the radiation field is small and $\vec{M}$ can be assumed to radiate in free space.

Under the assumption that the thickness h is very small compared to the free-space wavelength, the variation of E_x along the x direction can be neglected and the factor $e^{-j\beta x}$ in (1) can be suppressed. When the antenna resonates in the supported TM^x_{mn} mode, the electric field E is:

$$\vec{E} = \hat{x}E_x = \hat{x}E_0 \sin\left(\frac{m\pi y}{2W}\right)\sin\left(\frac{n\pi z}{L}\right)$$
$$m = 1, 3, 5\ldots \text{ and } n = 1, 2, 3\ldots \tag{6}$$

where E_0 is the electric field peak. The electric field only has the x-component and the theoretical electric field distributions for the TM^x_{11}, TM^x_{12}, and TM^x_{13} modes are plotted in Fig. 4. The equivalent magnetic current is obtained from E_x:

$$\overrightarrow{M} = -\hat{y} \times \overrightarrow{E_x}\,|_{y=W} = \hat{z}E_0 \sin\frac{n\pi z}{L}, \quad n = 1, 2, 3\ldots \tag{7}$$

The microstrip magnetic dipole antenna is closely related to the microstrip antenna. As shown in Fig. 5(a), the four radiating edges of a conventional rectangular microstrip antenna are equivalent to four linear magnetic currents, which produce a directional radiation due to the reflection of the ground plane. However, the microstrip magnetic dipole antenna has three shorting walls, only one radiating edge, and no reflective ground plane. Therefore, the microstrip magnetic dipole antenna is equivalent to a linear magnetic current. As shown

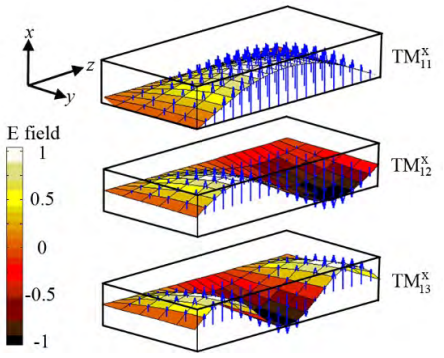

FIGURE 4. Theoretical electric field distributions for the TM^x_{11}, TM^x_{12} and TM^x_{13} modes of the microstrip magnetic dipole antenna.

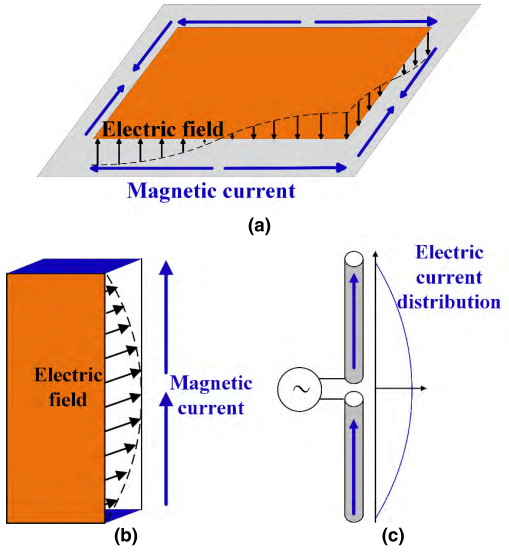

FIGURE 5. Relation between the rectangular microstrip antenna, the microstrip magnetic dipole antenna, and the electric dipole antenna. (a) Rectangular microstrip antenna. (b) Microstrip magnetic dipole antenna. (c) Electric dipole.

in Fig. 5(b) and Fig. 5(c), the microstrip magnetic dipole antenna is similar to the electric dipole antenna because both can be considered as radiating line sources with a sinusoidal distribution. Therefore, the microstrip magnetic dipole antenna produces a doughnut-shaped or conical radiation pattern similar to that of the electric dipole antenna.

Although the equivalent magnetic current (7) of the TM^x_{mn} mode is independent of m, the resonant wave number k in (4) depends on m and is used for the far-field calculation. When the TM^x_{mn}-mode far-field patterns of different resonant modes for the microstrip magnetic dipole are calculated, the width W needs to be adjusted according to the resonant wave number k:

$$W = \frac{m\pi}{2\sqrt{k^2 - (\frac{n\pi}{L})^2}} \tag{8}$$

Consequently, when the antenna length varies, the resonant mode at the fixed operating frequency $kc/2\pi$ remains unchanged.

According to Maxwell's equation with fictitious magnetic currents, the far-field electric field $\vec{E}_F$ can be obtained from the electric vector potential $\vec{F}$, which is calculated from an integral over the magnetic current:

$$\overrightarrow{E_F} = -\frac{1}{\varepsilon}\nabla \times \overrightarrow{F} = -\frac{jke^{-jkr}}{4\pi r}\hat{r} \times \int_0^L \overrightarrow{M}(z)e^{jk\overrightarrow{r}\cdot\overrightarrow{r'}} \quad (9)$$

where $\vec{r}$ is the measurement point radius vector and $\vec{r'}$ is the source point radius vector. The closed form expression of the far-field pattern for TM^x_{mn} mode is:

$$E_F(\theta) = \frac{jke^{-jkr}\sin\theta}{4\pi r} \cdot \frac{n\pi L(1 - e^{jkL\cos\theta}\cos n\pi)}{n^2\pi^2 - L^2k^2\cos^2\theta} \quad (10)$$

Fig. 6 shows the calculated far field patterns of a double-wavelength microstrip magnetic dipole antenna resonating in the TM^x_{11}, TM^x_{12}, and TM^x_{13} modes. A typical doughnut-shaped pattern, which is similar to that of a half-wavelength dipole, is produced by the TM^x_{11} mode. The main beam splits into conical beams when the antenna resonates in the TM^x_{12} and TM^x_{13} modes. The higher order mode produces conical beams with a smaller elevation angle.

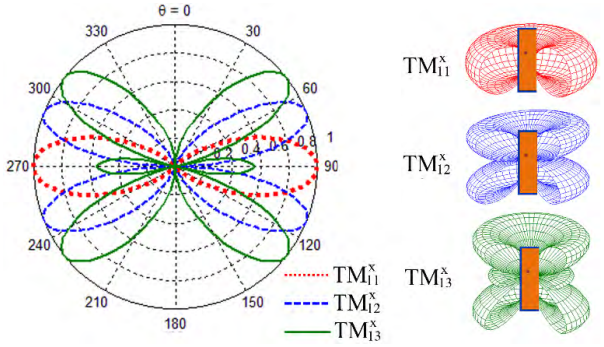

FIGURE 6. Calculated radiation patterns of a double-wavelength microstrip magnetic dipole antenna resonating in the TM^x_{11},TM^x_{12} and TM^x_{13} modes.

Fig. 7 shows the radiation patterns of the microstrip magnetic dipole antenna with various lengths resonating in a fixed mode. When the antenna resonates in the TM^x_{11} mode, the main beam remains in the azimuth plane for $\theta = 90°$ and becomes narrower as the antenna length increases. The conical beams produced by the TM^x_{12} and TM^x_{13} modes are tilted close to the *x*-*y* plane with the increase in the antenna length.

The main-beam elevation angle is obtained from the far-field results of the close form expression (10) and is shown in Fig. 8. If the antenna resonates in the TM^x_{12} mode, the elevation angle of the conical beam increases from 58° to 72° when the antenna length increases from λ to 2λ. Similarly, if the antenna resonates in the TM^x_{13} mode, the elevation angle of the main beam increases from 36° to 55° when the length increases from λ to 2λ. Therefore, it is possible to produce conical beams with various elevation angles if we can switch the resonant mode of the microstrip magnetic dipole antenna.

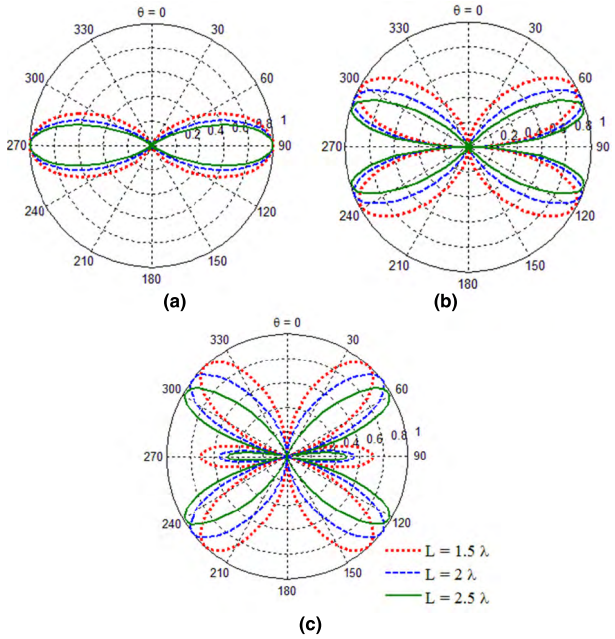

FIGURE 7. Calculated radiation patterns of microstrip magnetic dipole antennas with various lengths. (a) TM^x_{11} mode. (b) TM^x_{12} mode. (c) TM^x_{13} mode.

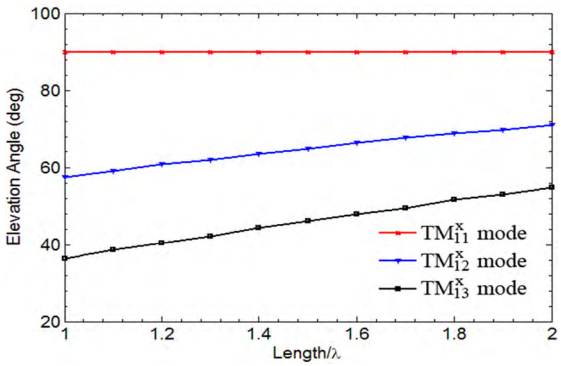

FIGURE 8. Calculated elevation angle of the main beam produced by the microstrip magnetic dipole antenna with varying lengths.

According to (5), the resonant frequencies (f^{TM}_{11}, f^{TM}_{12}, and f^{TM}_{13}) of the TM^x_{11}, TM^x_{12}, and TM^x_{13} modes are calculated for a microstrip magnetic dipole antenna with a fixed width of 0.25 wavelength. The results in Fig. 9 show that the higher order mode produces a higher resonant frequency but the resonant frequency decreases as the antenna length increases. Therefore, the resonant mode at a fixed frequency can be switched to a higher order mode when the antenna length increases. To vary the length of the microstrip magnetic dipole antenna, we can divide the antenna into several sub-cavities with shorting posts as shown in Fig. 10 and use RF switches to reconfigure the shorting posts. When different numbers of the sub-cavities are combined, the length of the resonant cavity varies and the resonant mode can be switched.

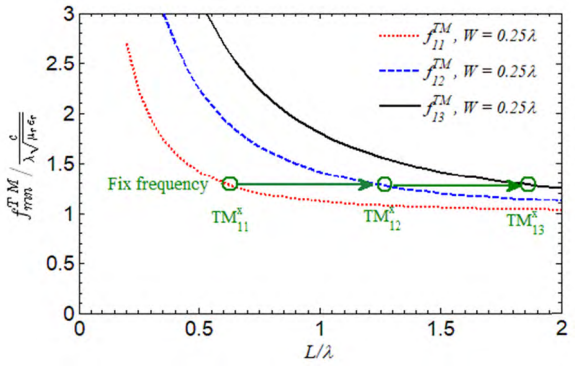

FIGURE 9. Calculated resonant frequencies of the microstrip magnetic dipole antenna with a width of 0.25 λ and varying lengths.

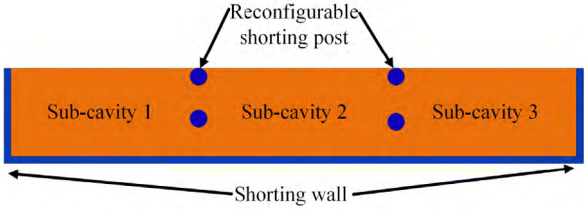

FIGURE 10. A microstrip magnetic dipole antenna with reconfigurable shorting posts.

III. ANTENNA CONFIGURATION

The geometry of the proposed antenna is shown in Fig. 11. This antenna is composed of two FR4 substrates with a thickness t of 1 mm, a relative dielectric constant of 4.4, and distance h of 4.8 mm. The shape of the substrate is a combination of three rectangles, the sizes of which are $L_1 \times W_1$ ($102\times33.8\text{mm}^2$), $L_2 \times W_2$($88\times33.8\text{mm}^2$), and $L_3 \times W_3$($62\times43\text{mm}^2$), respectively. Each substrate has a metal patch on the back, and the two metal patches are connected by shorting sidewalls to form a cavity. There are six shorting posts (a1, a2, a3, b1, b2, and b3) with a diameter of 1 mm. These posts are divided into two groups (Group#A and Group#B) and are connected to two DC biasing lines with voltages of DC#1 and DC#2. The shorting posts divide the proposed antenna into three rectangular sub-cavities (ABCD, CDEF, and EFGH). The shorting posts a2 and a3 are between the first and second cavity, and the shorting posts b2 and b3 are between the second and third cavity. These two pairs of posts have the same distance p of 16.8 mm. The shorting posts a1, a2, b1 and b2 are placed at the edge. The distance D_1 between a1 and a2 is 40 mm, and the distance D_2 between b1 and b2 is 25 mm. The ends of each shorting post are connected to the metal patches through an RF switch and a shorting via. Thus, direct current is blocked from reaching the metal patches. The RF switches connected to the shorting posts are also divided into two groups (Group#A and Group#B). A coaxial connector is used to feed the antenna. The feeding point is located in the first sub-cavity (ABCD) with distance W_f of 21 mm from the long sidewall and distance L_f of 72 mm from the short sidewall.

To reconfigure the resonant cavity of the antenna, we use PIN diodes (Infineon Bar50-02L [23]) as RF switches. Fig. 12 shows the equivalent circuit of the PIN diodes. When the diode is forward biased, it acts as a short circuit. The equivalent circuit of the diode in the RF band is a small parasitic inductance L_s (0.4 nH) in series with a small forward resistance R_1 (2 ohm). On the other hand, the diode will act as an open-circuit if it is in the OFF state. In this state, the equivalent circuit has the same parasitic inductance L_s (0.4 nH) in series with a large reverse resistance R_2 (5K ohm) and a small reverse capacitance C_p (0.1 pF) in parallel.

The operating states can be switched by changing the ON/OFF status of each group of the diodes as shown in Table 1. In order to obtain a fixed resonant frequency (2.44 GHz) for different resonant modes (TM^x_{11}, TM^x_{12}, and TM^x_{13} modes) in three operating states, we design the three sub-cavities one by one. The design process is separated into three steps.

First, we switch on all the PIN diodes to block the second and third cavities (CDEF and EFGH) in State I. Thus, only the first cavity (ABCD) needs to be designed by adjusting its length and width to obtain the TM^x_{11} resonant frequency at 2.44 GHz. Second, the PIN diodes of Group#A are switched off and the first and second cavity are combined. By adjusting the size of the second cavity, the TM^x_{12} resonant frequency in State II can be tuned in the same manner as the TM^x_{11} resonant frequency in State I. Finally, the size of the third cavity can be determined as in the second step. The optimized size parameters are listed in Table 2.

TABLE 1. Different operating states of the proposed antenna.

	DC#1	DC#2	Group#A	Group#B	Resonant Cavity	Resonant Mode
State I	3V	3V	ON	ON	ABCD	TM^x_{11}
State II	0V	3V	OFF	ON	ABEF	TM^x_{12}
State III	0V	0V	OFF	OFF	ABGH	TM^x_{13}

TABLE 2. Size parameters of the proposed antenna.

L_1	102 mm	L_2	88 mm	L_3	62 mm
L_f	72 mm	W_1	33.8 mm	W_3	43 mm
p	16.8 mm	W_2	33.8 mm	D_1	40 mm
D_2	25 mm	W_f	21 mm	t	1 mm
h	4.8 mm	d	0.8 mm		

IV. PARAMETRIC ANALYSIS

The simulated electric field is shown in Fig. 13 to distinguish the resonant modes. The proposed antenna operates in the TM^x_{11}, TM^x_{12}, and TM^x_{13} modes for State I, II and IIII, respectively. In this section, the effects of the key parameters for each operating state are discussed separately.

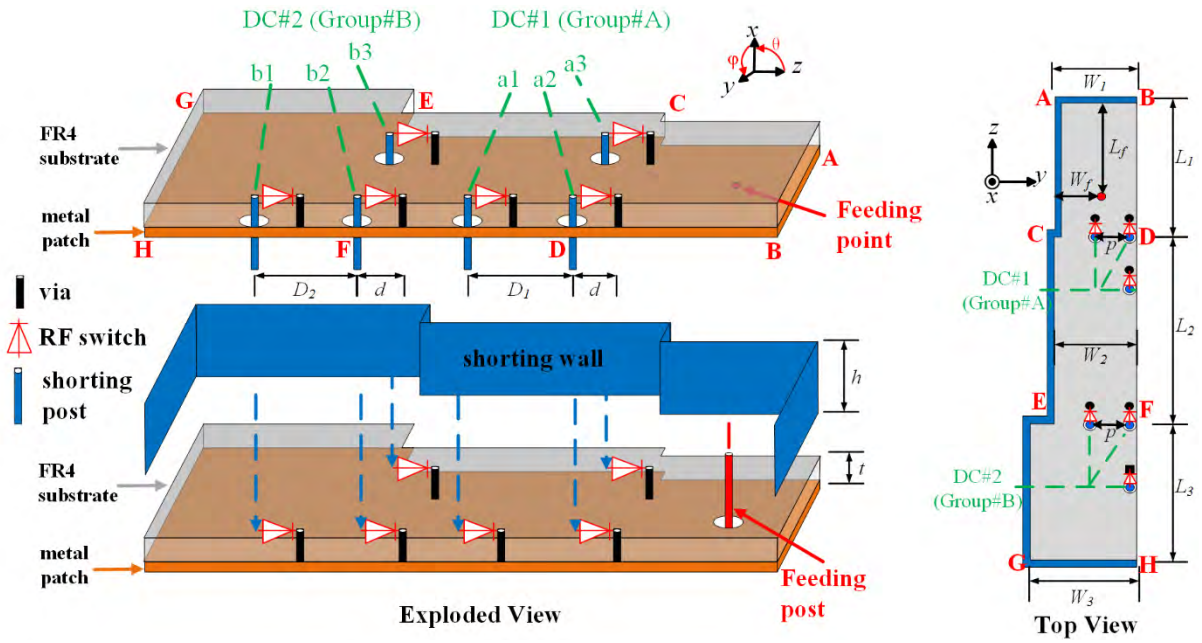

FIGURE 11. Geometry of the proposed antenna.

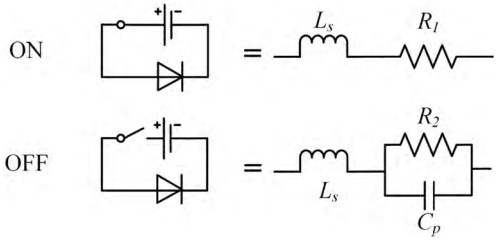

FIGURE 12. Equivalent circuit of the PIN diode (Infineon Bar50-02L) in different states.

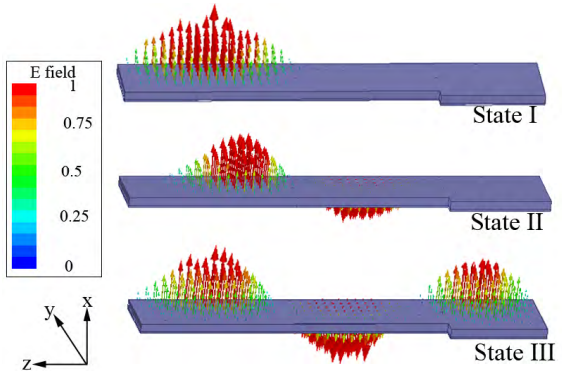

FIGURE 13. Simulated electric field of the proposed antenna in different operating states at 2.44 GHz.

A. STATE I WITH TM^x_{11} MODE

When all the diodes are switched on, the antenna is working in the first operating state (State I). In this state, the first cavity yields a resonant frequency of 2.44 GHz whereas the other cavities are shorted by the shorting posts. Fig. 13 shows the electric field of the antenna at 2.44 GHz for State I. A typical TM^x_{11} mode distribution similar to that in Fig. 4 is observed in the resonant cavity. The effect of the length L_1 and width W_1 on the resonant frequencies is shown in Fig. 14 and Fig. 15. The resonant frequency of the TM^x_{11} mode decreases when L_1 or W_1 increases. Therefore, the resonant frequency of State I can be tuned by adjusting L_1 and W_1. In addition, the impedance matching can be adjusted by varying the feeding position as shown in Fig. 16.

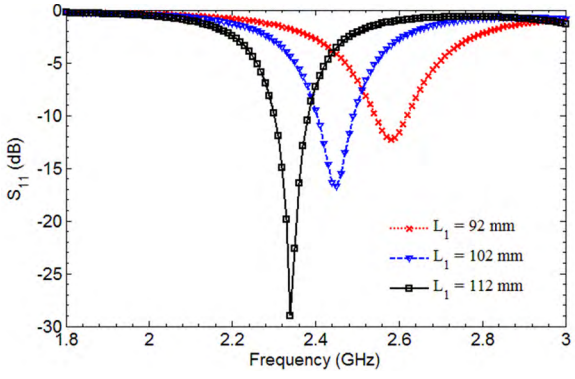

FIGURE 14. Simulated reflection coefficients of the proposed antenna in State I for different values of L_1.

B. STATE II WITH TM^x_{12} MODE

When the diodes of Group#A are turned off and those of Group#B are switched on, the two sub-cavities (ABCD and CDEF) are combined into a larger resonant cavity (ABEF). The larger cavity results in lower resonant frequencies. As shown in Fig. 17 and 18, the resonant frequencies decrease

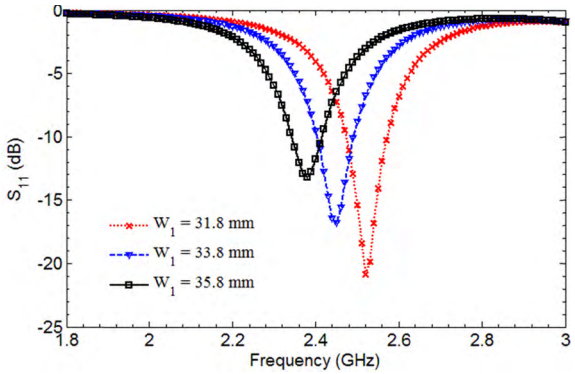

FIGURE 15. Simulated reflection coefficients of the proposed antenna in State I for different values of W_1.

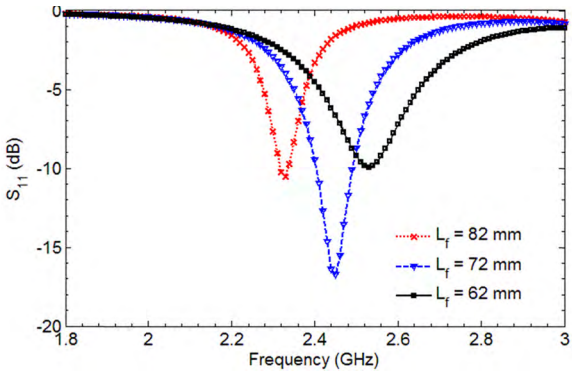

FIGURE 16. Simulated reflection coefficients of the proposed antenna in State I for different values of L_f.

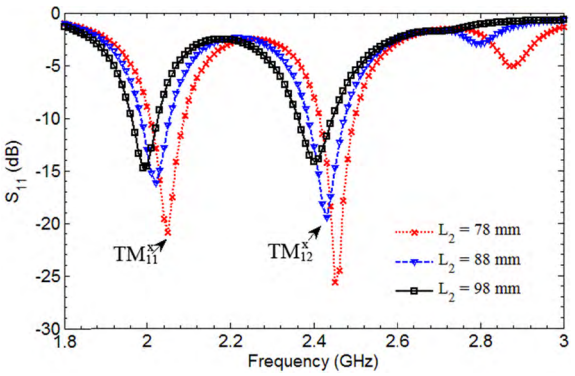

FIGURE 17. Simulated reflection coefficients of the proposed antenna in State II for different values of L_2.

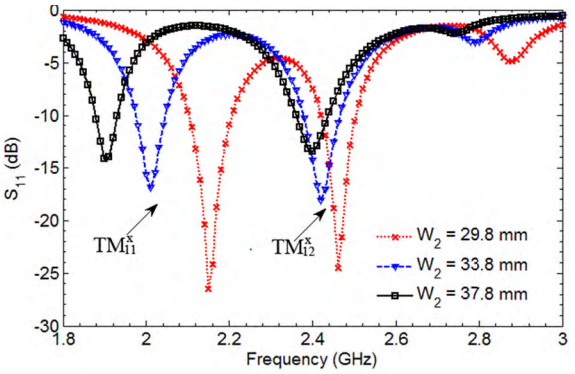

FIGURE 18. Simulated reflection coefficients of the proposed antenna in State II for different values of W_2.

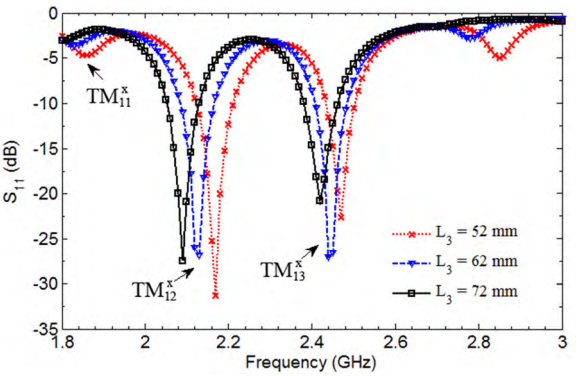

FIGURE 19. Simulated reflection coefficients of the proposed antenna in State III for different values of L_3.

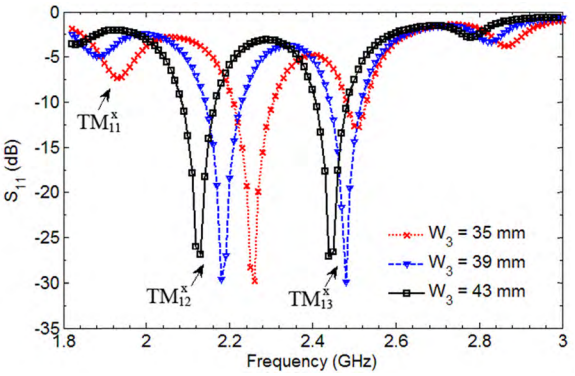

FIGURE 20. Simulated reflection coefficients of the proposed antenna in State III for different values of W_3.

as L_2 or W_2 increases. In this state (State II), the resonant frequency of TM^x_{11} mode drops to 2 GHz and the resonant frequency of TM^x_{12} mode becomes 2.44 GHz. As a result, the resonant mode of the antenna at 2.44 GHz is switched to the TM^x_{12} mode.

C. STATE III WITH TM^x_{13} MODE

When all the diodes are turned off, the three sub-cavities are combined together to cause further changes in the resonant frequencies. As shown in Fig. 19 and Fig. 20, all the resonant frequencies decrease as the length L_3 or width W_3 increases. In this operating state (State III), the resonant frequencies of the TM^x_{11} and TM^x_{12} modes drop to 1.8 GHz and 2.1 GHz respectively. The 2.44 GHz electric field distribution in Fig. 13 shows that the antenna is resonating in the TM^x_{13} mode for State III.

V. MEASUREMENT AND DISCUSSION

As shown in Fig. 21, a prototype has been fabricated, and its far-field is measured using the SATIMO StarLab

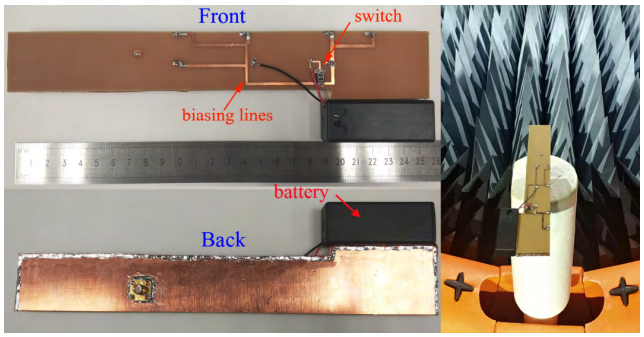

FIGURE 21. Prototype of the proposed antenna and its far-field measurement setup.

measurement system. The DC biasing lines and a switch are mounted on the front of the substrate. The DC biasing voltage of 3V is supplied by two 1.5 V batteries, which are mounted on the shorting wall. The biasing lines and batteries are placed outside the resonant cavity and the electric fields along the radiating edge are orthogonal to the biasing lines. Therefore, the presence of the biasing lines and batteries can be neglected. Fig. 22 shows the measured reflection coefficients of the proposed antenna in the three different states. In the first operating state, the antenna has a resonant frequency of 2.46 GHz. For State II, two resonant frequencies, which are obtained by the TM^x_{11} and TM^x_{12} modes respectively, are observed at 2.12 GHz and 2.42 GHz. For State III, three resonant frequencies of 1.90 GHz, 2.24 GHz, and 2.44 GHz are obtained. The overlap in the bandwidth of the three states ranges from 2.39 GHz to 2.49 GHz and covers the operating band of the WLAN 2.4 GHz applications.

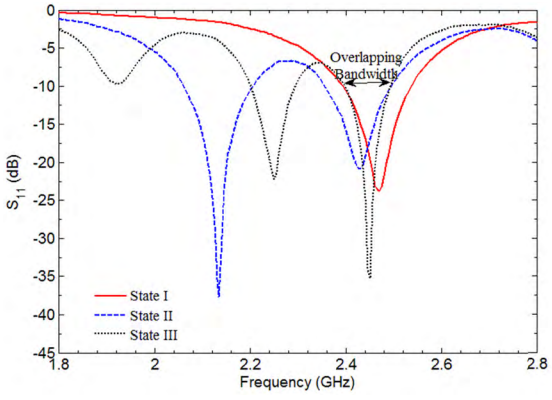

FIGURE 22. Measured reflection coefficients of the proposed antenna in different operating states.

The measured radiation patterns of State I, II, and III at 2.44 GHz are shown in Fig. 23, 24, and 25. Fig. 23 (b) and (c) show the doughnut-shaped radiation patterns which are similar to those of a conventional half-wavelength dipole. The simulated and measured patterns agree with the theoretical calculated results. An omnidirectional radiation pattern is produced in the azimuth plane for $\theta = 90°$. The shorting sidewall plays a role as an obstacle which causes diffraction.

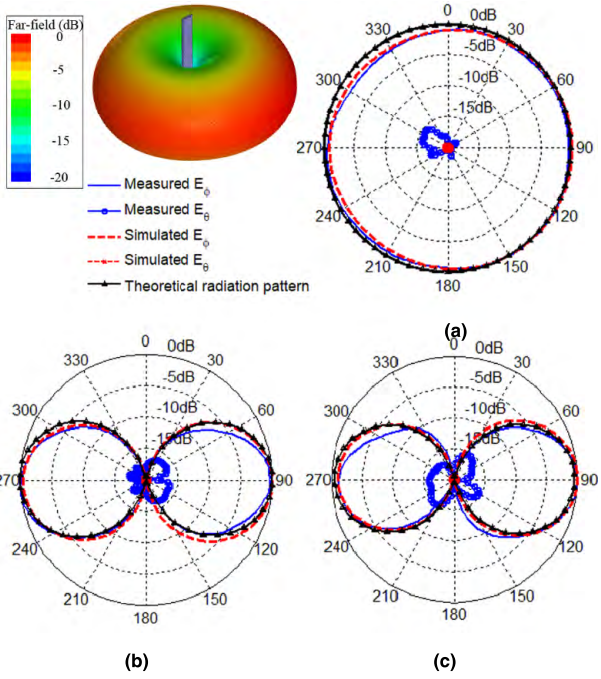

FIGURE 23. Radiation patterns of the proposed antenna in State I at 2.44 GHz. (a) The azimuth plane for $\theta = 90°$. (b) *x-z* plane. (c) *y-z* plane.

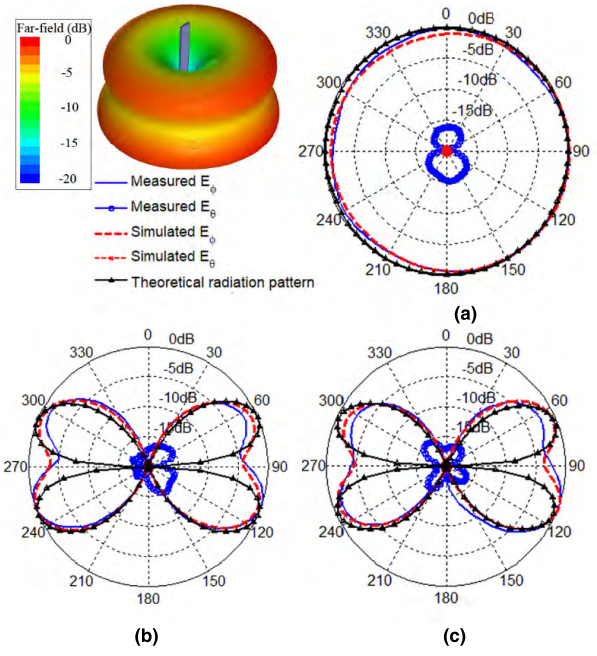

FIGURE 24. Radiation patterns of the proposed antenna in State II at 2.44 GHz. (a) The azimuth plane for $\theta = 114°$. (b) *x-z* plane. (c) *y-z* plane.

The diffraction of the shorting sidewall produces asymmetry in the azimuth radiation pattern. This asymmetry is slight because the diffraction effect of the shorting sidewall is negligible when its thickness is small. For State II, the main beam of the antenna splits into two conical beams as shown in Fig. 24 (b) and (c). Compared to the theoretical pattern, the simulated and measured down-tilted beams are slightly

stronger than the up-tilted beams. This behavior is caused by the asymmetry of the structure due to the feeding position. The down-tilted conical beam has an elevation angle of 66° and produces an omnidirectional radiation pattern in the azimuth plane for $\theta = 114°$ as shown in Fig. 24(a). For State III, the conical beams are further tilted away from the *x*-*y* plane ($\theta = 90°$) as shown in Fig. 25 (b) and (c). The difference between the up-tilted and down-tilted beams become apparent. The down-tilted conical beam has an elevation angle of 54° and yields an omnidirectional pattern in the azimuth plane for $\theta = 126°$. The antenna is horizontally polarized and its cross-polarization level is below −13 dB in all the operating states.

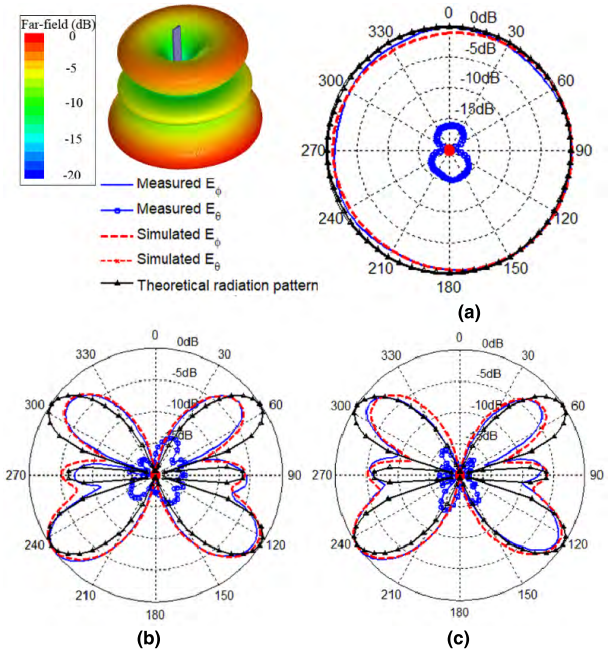

FIGURE 25. Radiation patterns of the proposed antenna in State III at 2.44 GHz. (a) The azimuth plane for $\theta = 126°$. (b) *x*-*z* plane. (c) *y*-*z* plane.

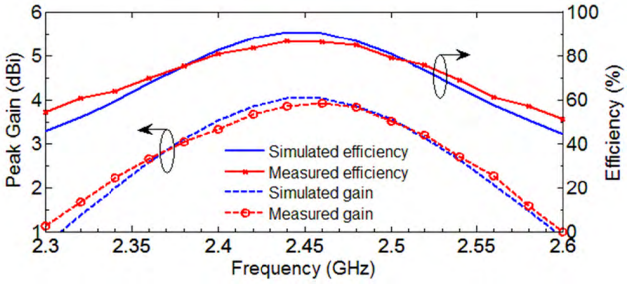

FIGURE 26. Efficiency and peak gain of the proposed antenna in State I.

The efficiency and peak gain of the proposed antenna in State I, II and III are shown in Fig. 26, 27 and 28, respectively. The average efficiency in the overlapping bandwidth is near 75% for all the operating states. The peak gain for State I, II, and III is 3.9, 4.0, and 4.3 dBi, respectively.

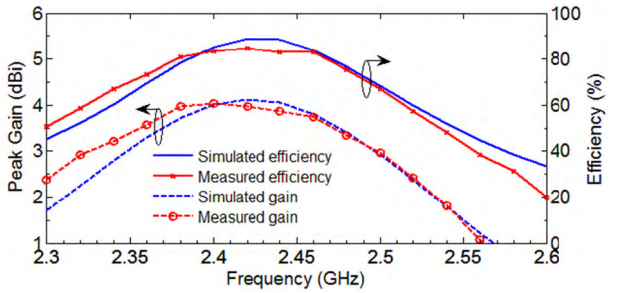

FIGURE 27. Efficiency and peak gain of the proposed antenna in State II.

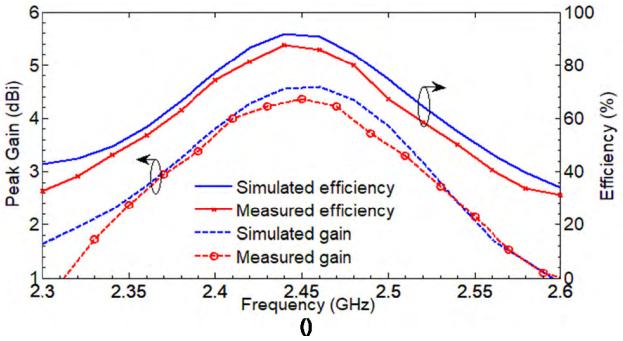

FIGURE 28. Efficiency and peak gain of the proposed antenna in State III.

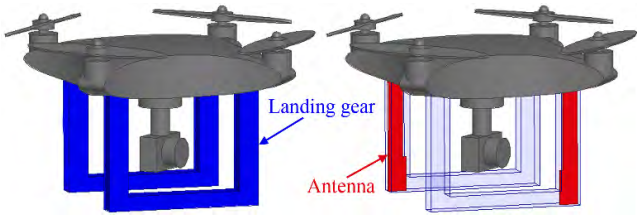

FIGURE 29. A 3D drone model with the proposed antenna integrated into the landing gear.

TABLE 3. Comparison between the proposed antenna and the existing reconfigurable antennas with conical beams.

Ref.	Bandwidth	Radiation modes	Main-beam elevation angle	Gain (dBi)	Size (λ_0^3)
[13]	2.5%	Broadside Conical	0° 50°	6.8 2.5	0.7×0.7 ×0.05
[14]	6.6 %	Broadside Conical	0° 45°	6.5 4.0	0.9×0.9 ×0.06
[15]	21.8%	Broadside Conical	0° 50°	9.9 3.8	1.1×1.1 ×0.12
[16]	23.5%	Broadside Conical	0° 30°	8.2 6.9	1.3×1.3 ×0.13
This work	4.0%	Conical Conical Conical	90° 66° 54°	3.9 4.0 4.3	2.0×0.4 ×0.06

The proposed antenna is compared to the existing reconfigurable antennas [13]–[16] with switchable conical beams. The performance of these antennas is summarized in TABLE 3. For the existing designs [13]–[16], there are only

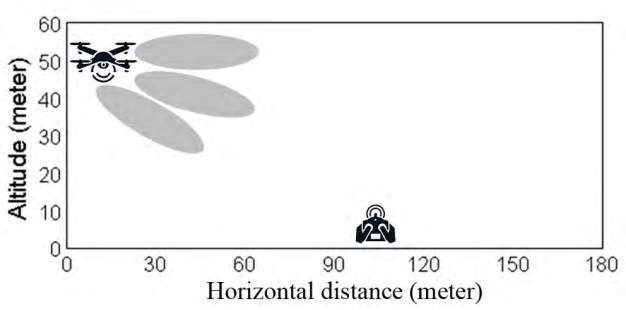

FIGURE 30. Scenario of an aerial drone with an antenna producing radiation beams with various elevation angles.

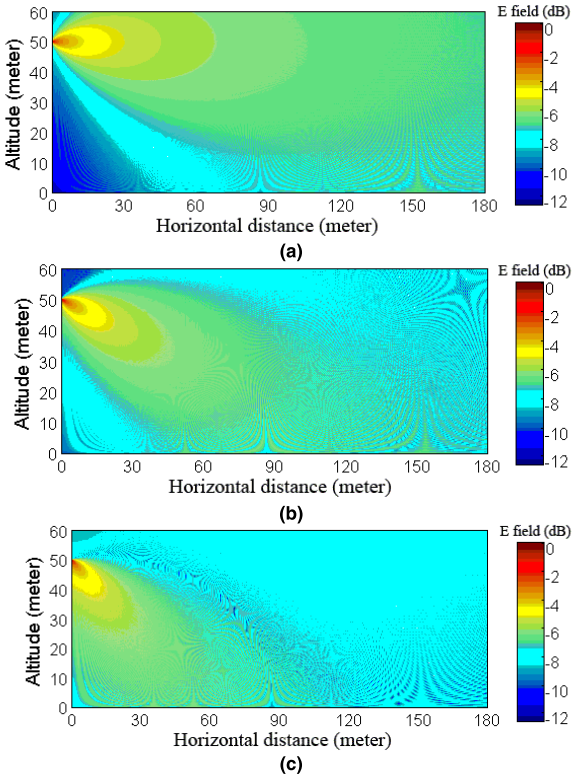

FIGURE 31. Wave propagation of a 2.4 GHz Gauss antenna at an altitude of 50 meters with a beamwidth of 30° and various elevation angles. (a) 90°. (b) 66°. (c) 54°.

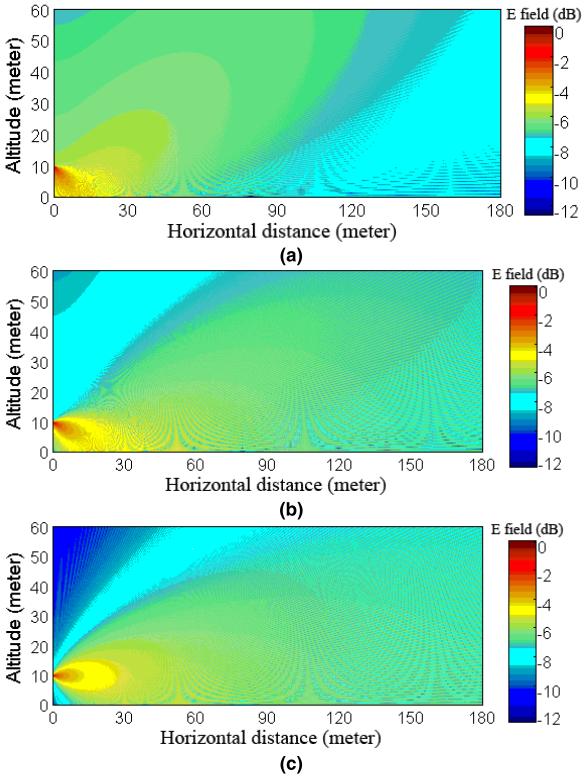

FIGURE 32. Wave propagation of a 2.4 GHz Gauss antenna at an altitude of 10 meters with a beamwidth of 30° and various elevation angles. (a) 54°. (b) 66°. (c) 90°.

two operating states (broadside and conical modes). Although the designs in [13]–[15] give higher gains in the broadside mode, the high gains are obtained for elevation angles below 30°. The small elevation angle limits the signal coverage on the ground. For the proposed antenna, there are three operating states, in which the conical beams with larger elevation angles of 54°, 66°, and 90° are produced. Therefore, the proposed antenna is more suitable for aerial drones operating at varying altitudes. Similar to the design in [13] and [14], the overlapping bandwidth of the proposed antenna has a narrow bandwidth of 4% due to its small thickness. It is capable of covering the operating band of WLAN 2.4 GHz applications. Although the proposed antenna is relatively long in the existing designs, it has a slender structure and can be integrated into the landing gear of drones as shown in Fig. 29.

To show the improvement of signal coverage due to the switchable beams, the geometrical optics method [24] is used to model the propagation of a radiating source producing a radiation beam with different elevation angles. The radiating source is modeled as a horizontally polarized Gaussian antenna pattern [25]:

$$f(\theta) = e^{-\ln 2 \cdot (\sin\theta - \sin\theta_{elev})^2 / 2\sin^2 \frac{\theta_{bw}}{2}} \tag{11}$$

where θ_{elev} is the elevation angle and θ_{bw} is the 3dB beamwidth. The ground is modeled as medium dry ground with a relative permittivity of 15 and a conductivity of 0.15 as per [26].

The wave propagation is calculated for the scenario of an aerial drone with a 2.4 GHz Gauss antenna ($\theta_{\text{bw}} = 30°$, $\theta_{\text{elev}} = 54°$, 66°, and 90°) located at a high altitude of 50 meters, as shown in Fig. 30. Fig. 31 (a), (b), and (c) show that the antenna provides the best coverage for the areas with different distances when the main-beam elevation angle changes.

The wave propagation for the scenario of an aerial drone located at a low altitude of 10 meters is also calculated. As shown in Fig. 32 (a), when the main-beam elevation angle is small, most of the radio wave is reflected to the sky. As a result, the coverage area on the ground is limited. In this

scenario, the coverage can be improved by increasing the elevation angle as shown in Fig. 32 (b) and (c).

For most commercial drones, horizontal distance can be estimated using GPS, and altitude can be estimated with barometric pressure and GPS data. The operating state of the proposed antenna can be switched according to the altitude and horizontal distance. When the drone is flying at a low altitude, State I is the best operating state to provide the largest coverage. When the drone is flying at a high altitude, State I, II, and III are suitable to cover the area at long distance, middle distance, and short distance, respectively.

VI. CONCLUSION

In this paper, we report on the development of a novel reconfigurable microstrip magnetic dipole antenna with switchable conical beams. The theoretical analysis reveals that microstrip magnetic dipole antennas produce conical beams with different elevation angles when they resonate in different modes. There are three operating states for the proposed antenna. By reconfiguring the resonant cavity of the antenna, it resonates at a fixed frequency of 2.44 GHz in the TM^x_{11}, TM^x_{12}, or TM^x_{13} modes. The overlap in the bandwidth of the three resonant modes ranges from 2.39 GHz to 2.49 GHz, which covers the WLAN 2.4 GHz band. The antenna produces switchable conical beams for different operating states. The peak gain is 3.9, 4.0, and 4.3 dBi, respectively when the elevation angle is 90°, 66°, and 54°. The proposed antenna shows promise for improving the transmission of aerial drones operating at varying altitudes.

REFERENCES

[1] Z. Li, E. Ahmed, A. M. Eltawil, and B. A. Cetiner, "A beam-steering reconfigurable antenna for WLAN applications," *IEEE Trans. Antennas Propag.*, vol. 63, no. 1, pp. 24–32, Jan. 2015.

[2] W.-Q. Deng, X.-S. Yang, C.-S. Shen, J. Zhao, and B.-Z. Wang, "A dual-polarized pattern reconfigurable Yagi patch antenna for microbase stations," *IEEE Trans. Antennas Propag.*, vol. 65, no. 10, pp. 5095–5102, Oct. 2017.

[3] M. Jusoh, T. Aboufoul, T. Sabapathy, A. Alomainy, and M. R. Kamarudin, "Pattern-reconfigurable microstrip patch antenna with multidirectional beam for WIMAX application," *IEEE Antennas Wireless Propag. Lett.*, vol. 13, pp. 860–863, 2014.

[4] T. Zhang, S.-Y. Yao, and Y. Wang, "Design of radiation-pattern-reconfigurable antenna with four beams," *IEEE Antennas Wireless Propag. Lett.*, vol. 14, pp. 183–186, 2014.

[5] A. Edalati and T. A. Denidni, "Frequency selective surfaces for beam-switching applications," *IEEE Trans. Antennas Propag.*, vol. 61, no. 1, pp. 195–200, Jan. 2013.

[6] M. Bouslama, M. Traii, T. A. Denidni, and A. Gharsallah, "Beam-switching antenna with a new reconfigurable frequency selective surface," *IEEE Antennas Wireless Propag. Lett.*, vol. 15, pp. 1159–1162, 2015.

[7] C. Gu *et al.*, "Frequency-agile beam-switchable antenna," *IEEE Trans. Antennas Propag.*, vol. 65, no. 8, pp. 3819–3826, Aug. 2017.

[8] R. O. Ouedraogo, E. J. Rothwell, and B. J. Greetis, "A reconfigurable microstrip leaky-wave antenna with a broadly steerable beam," *IEEE Trans. Antennas Propag.*, vol. 59, no. 8, pp. 3080–3083, Aug. 2011.

[9] D. K. Karmokar, K. P. Esselle, and S. G. Hay, "Fixed-frequency beam steering of microstrip leaky-wave antennas using binary switches," *IEEE Trans. Antennas Propag.*, vol. 64, no. 6, pp. 2146–2154, Jun. 2016.

[10] A. Suntives and S. V. Hum, "A fixed-frequency beam-steerable half-mode substrate integrated waveguide leaky-wave antenna," *IEEE Trans. Antennas Propag.*, vol. 60, no. 5, pp. 2540–2544, May 2012.

[11] S. V. S. Nair and M. J. Ammann, "Reconfigurable antenna with elevation and azimuth beam switching," *IEEE Antennas Wireless Propag. Lett.*, vol. 9, pp. 367–370, 2010.

[12] S.-J. Ha and C. W. Jung, "Reconfigurable beam steering using a microstrip patch antenna with a U-slot for wearable fabric applications," *IEEE Antennas Wireless Propag. Lett.*, vol. 10, pp. 1228–1231, 2011.

[13] S. H. Chen, J. S. Row, and K. L. Wong, "Reconfigurable square-ring patch antenna with pattern diversity," *IEEE Trans. Antennas Propag.*, vol. 55, no. 2, pp. 472–475, Feb. 2007.

[14] P.-Y. Qin, Y. J. Guo, A. R. Weily, and C.-H. Liang, "A pattern reconfigurable U-slot antenna and its applications in MIMO systems," *IEEE Trans. Antennas Propag.*, vol. 60, no. 2, pp. 516–528, Feb. 2012.

[15] L. Sun, G.-X. Zhang, B.-H. Sun, W.-D. Tang, and J.-P. Yuan, "A single patch antenna with broadside and conical radiation patterns for 3G/4G pattern diversity," *IEEE Antennas Wireless Propag. Lett.*, vol. 15, pp. 433–436, 2015.

[16] W. Lin, H. Wong, and R. W. Ziolkowski, "Wideband pattern-reconfigurable antenna with switchable broadside and conical beams," *IEEE Antennas Wireless Propag. Lett.*, vol. 16, pp. 2638–2641, 2017.

[17] J. Liu and Q. Xue, "Microstrip magnetic dipole Yagi array antenna with endfire radiation and vertical polarization," *IEEE Trans. Antennas Propag.*, vol. 61, no. 3, pp. 1140–1147, Mar. 2013.

[18] Y. Zhang, Z. Xue, J. Cao, W. Li, and W. Ren, "Research on arrays of microstrip magnetic dipole Yagi antennas," in *Proc. APCAP*, Jul. 2014, pp. 635–638.

[19] J. Liu, Y. Li, Z. Liang, and Y. Long, "A planar quasi-magnetic–electric circularly polarized antenna," *IEEE Trans. Antennas Propag.*, vol. 64, no. 6, pp. 2108–2114, Jun. 2016.

[20] F. Wu and K. M. Luk, "A compact and reconfigurable circularly polarized complementary antenna," *IEEE Antennas Wireless Propag. Lett.*, vol. 16, pp. 1188–1191, 2016.

[21] C. A. Balanis, *Advanced Engineering Electromagnetics*. New York, NY, USA: Wiley, 2012, ch. 8, pp. 351–389.

[22] D. M. Pozar, *Microwave Engineering*. New York, NY, USA: Wiley, 1998, ch. 3, pp. 100–103.

[23] *Data Sheet of Bar50-02L Pin Diodes, Infineon Technologies*, Appl. Note AN_1809_PL32_1810_172154. [Online]. Available: http://www.infineon.com/

[24] D. A. McNamara, C. W. I. Pistorius, and J. A. G. Malherbe, *Introduction to the Uniform Geometrical Theory of Diffraction*. London, U.K.: Artech House, 1990, ch. 8, pp. 331–337.

[25] A. E. Barrios, "A terrain parabolic equation model for propagation in the troposphere," *IEEE Trans. Antennas Propag.*, vol. 42, no. 1, pp. 90–98, Jan. 1994.

[26] A. E. Barrios and W. L. Patterson, "Advanced propagation model (APM) computer software configuration item (CSCI)," Space Naval Warfare Syst. Center, San Diego, CA, USA, Tech. Rep. 3145, Aug. 2002, p. 41.

ZHIXI LIANG (M'18) was born in Huizhou, Guangdong, China, in 1989. He received the B.S. degree in electronics information science and technology and the Ph.D. degree in radio physics from Sun Yat-sen University, Guangzhou, China, in 2011 and 2016, respectively, where he holds a postdoctoral position.

His current research interests include microstrip patch antennas, microstrip magnetic dipole antennas, and endfire antennas.

ZHIPENG LIANG was born in Huizhou, Guangdong, China, in 1996. He received the B.S. degree in electronics information science and technology from the Guangdong University of Technology, Guangzhou, China, in 2018.

He is currently pursuing the M.S. degree with Sun Yat-sen University, Guangzhou. His current research interests include microstrip patch antennas and computational electromagnetics.

YUANXIN LI (M'08) was born in Guangzhou, China. He received the B.S. and Ph.D. degrees from Sun Yat-sen University, China, in 2001, and 2006, respectively.

He was a Senior Research Assistant, from 2006 to 2008, and a Research Fellow, in 2010, with the State Key Laboratory of Millimeter Waves, City University of Hong Kong. In 2008, he joined the Department of Electronics and Communication Engineering, Sun Yat-sen University, where he is currently an Associate Professor. His current research interests include microstrip leaky-wave antennas and the applications of the periodic construction.

JUHUA LIU (M'12) was born in Heyuan, Guangdong, China, in 1981. He received the B.S. and Ph.D. degrees in electrical engineering from Sun Yat-sen University, Guangzhou, China, in 2004 and 2011, respectively.

From 2008 to 2009, he was a Visiting Scholar with the Department of Electrical and Computer Engineering, University of Houston, Houston, TX, USA. From 2011 to 2012, he was a Senior Research Associate with the State Key Laboratory of Millimeter Waves, City University of Hong Kong, Hong Kong. From 2012 to 2015, he was a Lecturer with the Department of Electronics and Communication Engineering, Sun Yat-sen University, where he has been an Associate Professor, since 2015. His research interests include microstrip antennas, substrate-integrated waveguide antennas, leaky-wave antennas, periodic structures, and computational electromagnetics.

JIAYIN QIN received the M.S. degree in radio physics from Huazhong Normal University, China, and the Ph.D. degree in electronics from Sun Yat-sen University (SYSU), Guangzhou, China, in 1992 and 1997, respectively.

Since 1999, he has been a Professor with the School of Information Science and Technology, SYSU. From 2002 to 2004, he was the Head of the Department of Electronics and Communication Engineering, SYSU. From 2003 to 2008, he was the Vice Dean of the School of Information Science and Technology, SYSU. His research interests include wireless communication and submillimeter-wave technology. He was a recipient of the IEEE Communications Society Heinrich Hertz Award for the Best Communications Letter, in 2014, the Second Young Teacher Award of Higher Education Institutions, Ministry of Education (MOE), China, in 2001, the Seventh Science and Technology Award for Chinese Youth, in 2001, and the New Century Excellent Talent, MOE, China, in 1999.

YUNLIANG LONG (M'01–SM'02) was born in Chongqing, China. He received the B.Sc., M.Eng., and Ph.D. degrees from the University of Electronic Science and Technology of China, Chengdu, in 1983, 1989, and 1992, respectively.

From 1992 to 1994, he was a Postdoctoral Research Fellow and, then, an Associate Professor with the Department of Electronics, Sun Yat-sen University, Guangzhou, China. From 1998 to 1999, he was a Visiting Scholar with the IHF, RWTH University of Aachen, Germany. From 2000 to 2001, he was a Research Fellow with the Department of Electronics Engineering, City University of Hong Kong, Hong Kong. He is currently a Full Professor and the Head of the Department of Electronics and Communication Engineering, Sun Yat-sen University. He has authored or co-authored over 200 academic papers. His research interests include antennas and propagation theory, EM theory in inhomogeneous lossy medium, computational electromagnetics, and wireless communication applications.

Dr. Long is a member of the Committee of Microwave Society of CIE. He serves on the Editorial Board of the *Chinese Journal of Radio Science*. He is the Vice Chairman of the Guangzhou Electronic Industrial Association.